medRxiv preprint doi: https://doi.org/10.1101/2022.07.26.22277593; this version posted July 27, 2022. The copyright holder for this preprint (which was not certified by peer review) is the author/funder, who has granted medRxiv a license to display the preprint in perpetuity.
All rights reserved. No reuse allowed without permission.

COMPARATIVE ANALYSIS OF THREE MACHINE LEARNING MODELS FOR EARLY PREDICTION OF SKELETAL CLASS-III MALOCCLUSION FROM PROFILE PHOTOS

Banu KILIÇ**, Department of Orthodontics, Bezmialem Vakif University, Turkey, bkilic@bezmialem.edu.tr
(https://orcid.org/0000-0002-9207-4490-ORCID NO)
Tuğba ÖNAL-SÜZEK*, Department of Bioinformatics, Muğla Sıtkı Koçman University, Turkey, tugbasuzek@mu.edu.tr
(https://orcid.org/0000-0002-3243-1759-ORCID NO)
Selahattin AKSOY**, Department of Bioinformatics, Muğla Sıtkı Koçman University, Turkey, selahattinaksoy@mu.edu.tr
(https://orcid.org/0000-0002-2574-7237-ORCID NO)

Received: XX.XX.20XX, Accepted: XX.XX.20XX
Research Study
*Corresponding author
**These authors contributed equally
DOI: 10.5505/jmst.2012.XXXXX

Abstract

The pre-adolescent growth period is the best time for the skeletal Class-III malocclusion treatment. Diagnosis and treatment during this period continue to be a complex orthodontic problem. Class-III malocclusion is complicated to treat with braces frequently requiring surgical intervention after a pubertal growth spurt. In addition, delayed recognition of the problem will yield significant functional, aesthetic, and psychological concerns. This study presents the first fully automated machine learning method to accurately diagnose Class-III malocclusion applied across mobile images, to the best of our knowledge. For this purpose, we comparatively evaluated three machine learning approaches: a deep learning algorithm, a machine learning algorithm, and a rule-based algorithm. We collected a novel profile image data set for this analysis along with their formal diagnosis from 435 orthodontics patients. The most successful method among the three was the machine learning method, with an accuracy of %76.

Keywords: Class-III Malocclusion, Machine Learning, Medical Informatics

Cite

Aksoy S,Kılıç B,Önal-Süzek T(2022). "Comparative Analysis of Deep Learning and Machine Learning Models for Early Prediction of Skeleton Class-III Malocclusion from Profile Photos".

1. Introduction

Skeleton Class-III malocclusion is characterized by the sagittal developmental retardation and/or rearward positioning of the maxilla or the extreme development and/or forward positioning of the mandible [1]. Class-III malocclusion causing a concave profile causes aesthetic anxiety in the child and the parents [2]. The correction of the harmony between the mandible and maxilla can be provided by orthodontic/orthopedic appliances to be performed in early terms on the patients affecting the active sutures unclosed. Although the ideal age of treatment with orthopedic devices is preferably eight at the latest, it has also been reported that they can be effective up to 12 years of age [3]. It has been shown that early Class-III orthopedic treatment reduces the need for orthognathic surgery [4]. The American Association of Orthodontists (AAO) recommends that all children be checked by an orthodontist no later than age seven. However, the most common age group during which patients seek orthodontic treatment is 12 years and older [5]. Moreover, many children do not have access to an orthodontic pre-examination at seven and before. Advances in consumer electronics and portable communications systems, particularly mobile phones, have

NOTE: This preprint reports new research that has not been certified by peer review and should not be used to guide clinical practice.

medRxiv preprint doi: https://doi.org/10.1101/2022.07.26.22277593; this version posted July 27, 2022. The copyright holder for this preprint (which was not certified by peer review) is the author/funder, who has granted medRxiv a license to display the preprint in perpetuity. All rights reserved. No reuse allowed without permission.

led to faster and less expensive approaches to developing Point of Care Diagnosis[6]. Number of mobile subscribers globally according to GSMA Intelligence 2021 data reached approximately 5.22 billion [7]. Triggered by the Covid-19 pandemic period, the tele-health industry and more specifically the mobile health industry has become a 100 billion dollar market by increasing five times since 2016 as of the end of 2021 [8]. There are several dental mobile applications in the current healthcare mobile application market [9]. Current applications are mainly developed for patient education about general dentistry [10], braces, Invisalign (Align Technology, San Jose, Calif), and oral health [11]. The commercial software Phimentum[12] claims using deep-learning for automatic landmark point detection on cephalometric images. Unlike Phimentum, our program has the advantage of not requiring cephalometric image input and/or an orthodontist's supervised selection of landmark points can compute the probability of Class-III diagnosis without any other apparatus other than mobile phones.

Our previous study [13], implemented an unsupervised diagnostic method based on the angles computed for Turkish adult patients [14]. Our previous study's disadvantage was that it was only applicable to Turkish adult patients. Our present study aimed to compare the accuracies of three alternative unsupervised machine learning approaches for malocclusion diagnosis. Best performing model of three will be adaptable to be trained on any given image set of any race or age rather than a fixed threshold determined for Turkish patients. For this purpose, we implemented and presented the accuracies of three methods; deep- learning algorithm, a machine learning algorithm, and a rule-based algorithm for an in-house image data set we collected from orthodontics patients.

2. Collection of Data

The data set created within the project's scope consists of profile photos of patients visiting Orthodontics at Bezmialem Vakıf University Faculty of Dentistry. The Institutional Review Board approval (IRB# 54022451-050.05.04) was obtained from Bezmialem Vakıf University to use profile image data of patients who applied to Bezmialem Vakıf University in our project. The orthodontist with 20 years of orthodontics clinical experience diagnosed the patient images and classified them into three classes, Class-I, II, and III using Dolphin Imaging software (Version 11.95). The profile image taken for each patient is saved with an anonymized name in JPG/PNG format. Our anonymized dataset consists of 435 profile images and with their formal diagnosis from the orthodontics clinic.

3. Materials and Methods

Three alternative methods, namely the Rule-based , Deep Learning, and Machine Learning methods were implemented (Fig-1).

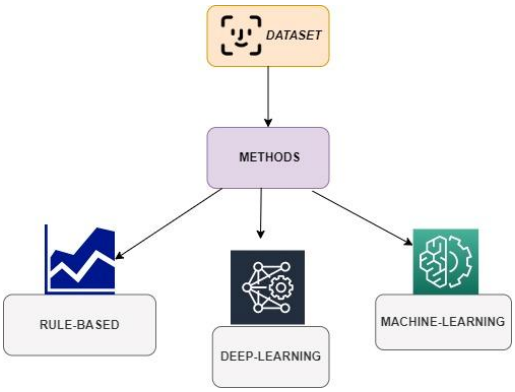

Figure 1. Flow-chart of the implemented pipeline

In this three methods we used mainly python programming language and it's libraries scikit-learn for Machine Learning approach, OpenCV for image processing and pandas , seaborn etc. libraries for visualization and data analysis. In addition to that we used Tensorflow-Keras for deep learning approach. We used script base complier to run our python codes and other required python libraries.

3.1. Deep Learning Approach

For Deep Learning Method, firstly, the images were pre-processed, and then the deep learning model was created.

medRxiv preprint doi: https://doi.org/10.1101/2022.07.26.22277593; this version posted July 27, 2022. The copyright holder for this preprint (which was not certified by peer review) is the author/funder, who has granted medRxiv a license to display the preprint in perpetuity.
All rights reserved. No reuse allowed without permission.

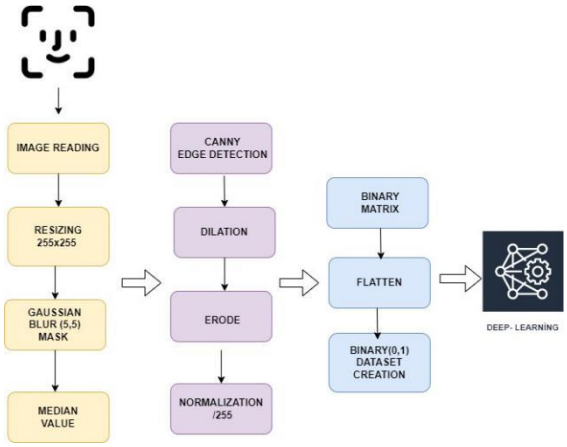

Figure 2. Image processing pipeline.

The images were first converted to gray-scale using the Python Open-CV library. Each image was scaled to 255X255 to standardize the images. Gaussian filtering was applied to scaled images using a 5x5 kernel matrix using OpenCV. Gaussian filtering (Gaussian Blur) was applied to reduce the noise and detail. Then, the median values were computed for each picture. With these median values, the contours of the profile images were extracted using OpenCV “Canny Edge detection” on each picture. Using dilation (Spreading and Expansion) and erosion operations pixels were added to the silhouette to make them more prominent. We applied dilation to expand the borders; thanks to this expansion, we enlarged the pixel groups and reduced the spaces between the pixels.

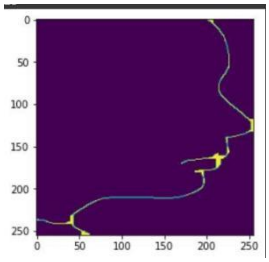

Figure 3. Silhouette output of the deep-learning pre-processing.

Next, the images were normalized using the min-max normalization formula (Fig-4), as all the images have a matrix with pixel values (0,255). As a result of this process, we converted our pictures into binary (0,1) form. Afterwards, we converted our matrix into a one-dimensional list by applying Flatten in order to use the 2D picture matrices we obtained in deep learning. As a result each picture’s silhouette, (Fig-3) was acquired in a single dimension.

$$x' = \frac{x - \min(x)}{\max(x) - \min(x)}$$

Figure 4. Normalization formula.

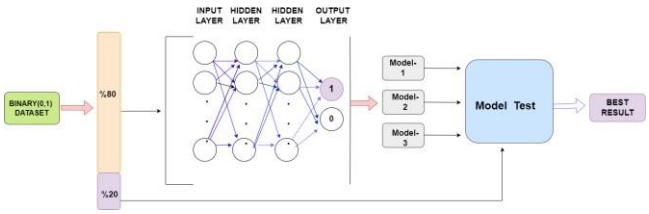

Figure 5. Deep learning model used.

The images were split into 80% training and 20% test set. 80% of the images were used for training the deep- learning model. Our deep learning model used a 4- layer structure, an input layer, two hidden layers, and an output layer. Since we were aiming a binary classification, we used "Relu" as the activation function in our input layer, and we used the sigmoid function in the intermediate layers. We used "Adam" as the optimizer and "cross entropy" as the optimizer loss function.

Table 1. Accuracy of the deep learning method.

Accuracy	**0.7090909090909091**
Precision	**0.6470588235294118**
F1	**0.5789473684210527**
Recall	**0.5238095238095238**
AUC	**0.6736694677871147**

After creating the training model, we tested our model with our independent test data. As a result, a deep- learning model with 70% accuracy and 64% sensitivity was created for the disease classification. As a higher accuracy was required for a clinical setting, we experimented with additional unsupervised methods that do not require a pre-set angle coefficient for diagnosis. To achieve this goal, we implemented the rule based method as the next step.

medRxiv preprint doi: https://doi.org/10.1101/2022.07.26.22277593; this version posted July 27, 2022. The copyright holder for this preprint (which was not certified by peer review) is the author/funder, who has granted medRxiv a license to display the preprint in perpetuity.
All rights reserved. No reuse allowed without permission.

3.2 Rule Based Approach

The same re-sizing and pre-processing steps were carried out for the critical value method on the images. Using the Python face-alignment library [15], 68 facial landmark points were selected., Po', Sn', A', Ls, Li, B, Pg', and Gn' were determined among these landmarks. After determining the other points requested by the orthodontist (Fig-6), the area between the Po' point at ear level and the area surrounding the Li (Lower Lip) part green area in Fig-7) and the remaining area between Ls - Sn'- Po' (red zone in Fig-7) Python OpenCV After masking, the ratio of the regions were computed in pixels.

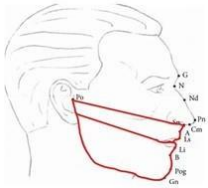

contact author for this image

Figure 6. Two regions compared.

Figure 7. Two regions compared.

Table 2. Descriptions of facial landmarks.

Abbreviations	Definitions
N'	Soft tissue Nasion. Midpoint on the soft tissue contour of the base of the nasal root at the level of the frontonasal suture.
Ls	Labialis superior; the most anterior point of the upper lip.
Li	Labialis inferius: The most anterior point of the lower lip
Pg'	Soft tissue pogonion. The most anterior point on the mandible in the midline; the most anterior, prominent point on the chin.
Po'	Soft tissue porion : most superior point of the external acoustic meatus.
Pn	Pronasale; The tip of the nose.
Sn'	Soft tissue subnasal: The point at which thenasal septum merges with the uppercutaneous lip in the midsagittal plane.
A'	Soft tissue A point; The outer point of intersection between the A point horizontal line and the soft tissue.
B'	Soft tissue B point; The outer point of intersection between the B point horizontal line and the soft profile.
Soft Tissue Facial Plane	Line between soft tissue nasion to soft tissue pogonion
H line	Harmony line: drawn tangent to the soft tissue chin and the upper lip.
H angle	The angle formed between the softtissue facial plane line and the H line

For the area ratios of all patients, a total of 435 images, 162 Class-I, 163 Class-II, and 110 Class-III, we first plotted the descriptive statistical analysis and visualization.

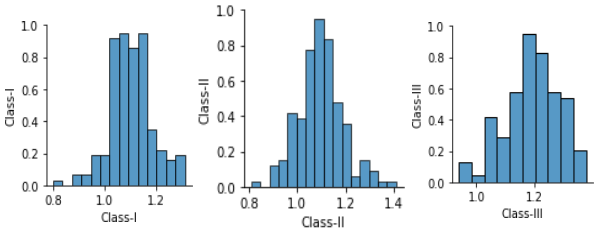

Figure 8. Histogram of each class showing the normalized number of samples.

Histogram graphs were plotted to show the distribution of each class; Class-I, Class-II, and Class-III (Fig-8). As seen in the histograms there is no left or right skewness (Left-Right Skewed Distribution) and the data show a normal distribution

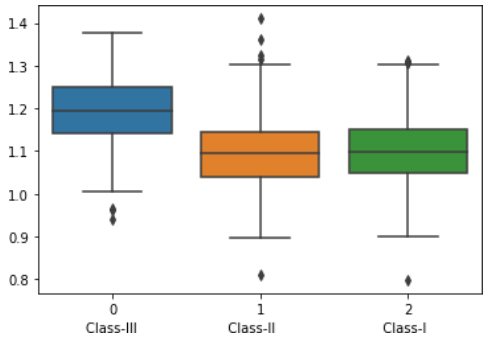

Figure 9. Boxplots of Class-I, Class-II, and Class-III.

The boxplots of the three classes in Fig-9 imply that the area ratios of Class-III patients were distinctly different from the other classes. Outliers in the boxplot were filtered and checked for misdiagnosis.

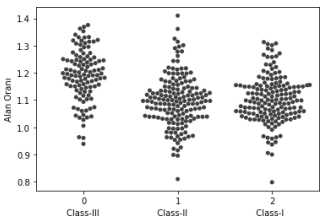

Figure 10. Scatter plot.

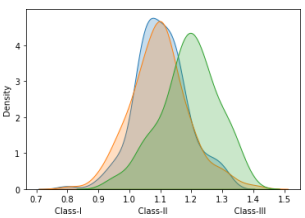

Figure 11. Density plot.

medRxiv preprint doi: https://doi.org/10.1101/2022.07.26.22277593; this version posted July 27, 2022. The copyright holder for this preprint (which was not certified by peer review) is the author/funder, who has granted medRxiv a license to display the preprint in perpetuity.
All rights reserved. No reuse allowed without permission.

In Fig-10, scatter plot of the patients also shows that Class-III patients have distinct area ratio values. As seen in the density plot in Fig-11, the area values showed a normal distribution for all classes yet the mean of the Class-III area ratio was higher than the other two classes.

3.2.1. Evaluation of Class-III vs not

Classification of area ratios for our goal, we designed binary classification experiment of Class-III and not Class-III. In this setting, 110 patients were Class-III and 325 patients were not Class-III (Fig-12).

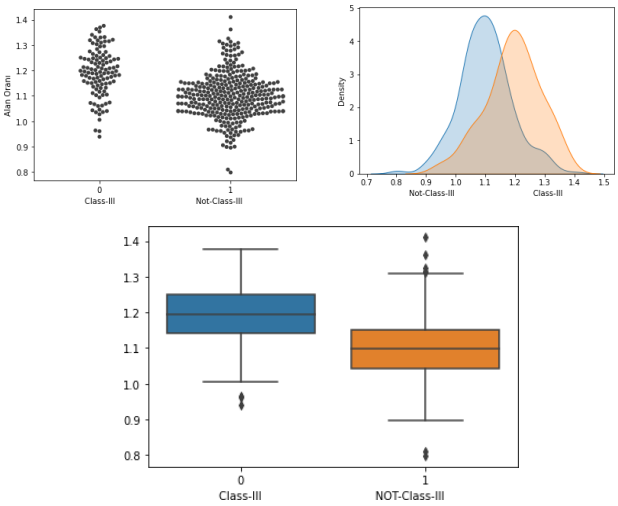

Figure 12. Distributions of Class-III and non-Class-III.

The area ratios of Class-III and non-Class-III followed a normal distribution (Figure 12-13).

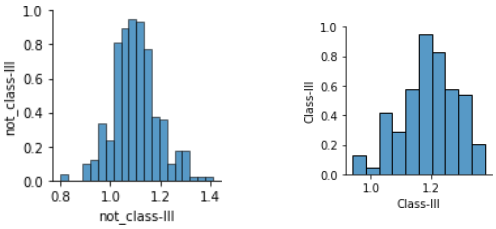

Figure 13. Histograms of Class-III and non-Class-III.

3.2.2. Cleaning Up Outliers

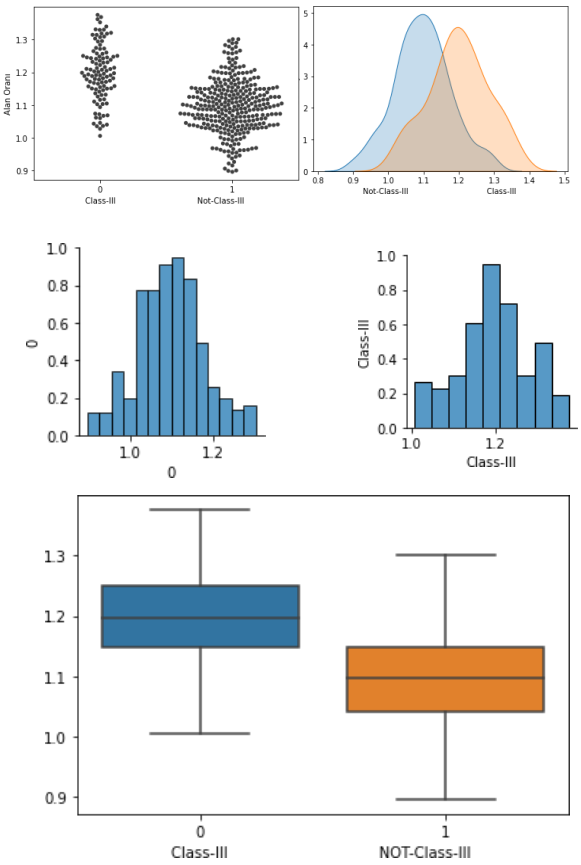

Figure 14. Plots of Class-III and non-Class-III after cleaning outliers.

Outliers were detected using the formula of Interquartile range (IQR) [Q1- 1.5*IQR -Q3+1.5*IQR], we found 12 outliers and removed them from the dataset. We obtained a total of 423 patients. We repeated the analysis as in Fig-14.

3.2.3 Experimental Setup

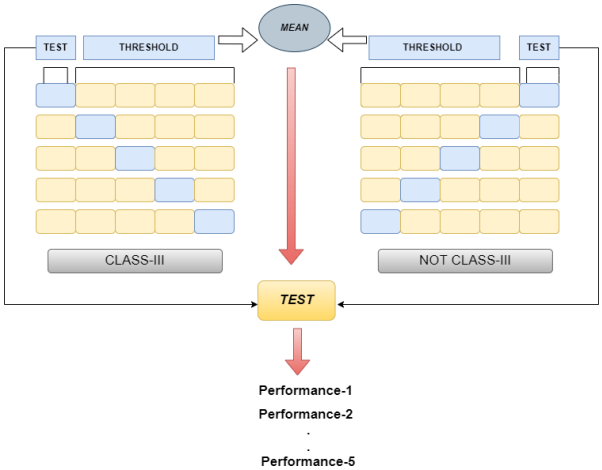

Figure 15. Experimental set up for classification.

medRxiv preprint doi: https://doi.org/10.1101/2022.07.26.22277593; this version posted July 27, 2022. The copyright holder for this preprint (which was not certified by peer review) is the author/funder, who has granted medRxiv a license to display the preprint in perpetuity.
All rights reserved. No reuse allowed without permission.

To check whether the distinct area ratio difference of Class-III is random or not, we have created an experimental setup (Fig-15) in the form of a critical value (threshold). In the experiment setup, we divided the Class-III and non-Class-III data into 5 parts with 5- fold separately, and the average of 4 parts of the data set was labeled training. The same process was repeated for the non-Class-III dataset. The resulting rule-based value was tested with the independent test dataset of Class-III and non-Class-III data. The process was repeated for the entire 5-fold. The classification was labeled not Class-III if the test data area ratio was greater than the critical value and Class-III if it was less than the critical value. As a result of classification

Precision = TP/(TP+FP)
Recall = TP/(TP+FN)
F1= 2*(Recall * Precision) / (Recall + Precision)
Specificity =TN/(TN+FP)
Accuracy = (TP+TN)/(TP+FP+FN+TN)

TP = True Positive TN = True Negative
FP = False Positive FN = False Negative

3.2.4. Results

Table 3. The result of the experiment (3.2.3) for the whole data set.

	Accuracy	Recall	Precision	F1	Specificity
Fold- 1	0.712644	0.636364	0.451613	0.528302	0.738462
Fold- 2	0.735632	0.727273	0.484848	0.581818	0.738462
Fold- 3	0.666667	0.772727	0.414634	0.539683	0.630769
Fold- 4	0.758621	0.863636	0.513514	0.644068	0.723077
Fold- 5	**0.793103**	0.727273	0.571429	0.640000	0.815385
Mean	0.733333	0.745455	0.487208	0.586774	0.729231
STD	0.042637	0.073855	0.053525	0.048532	0.058865

We shuffled our experimental dataset 100 times to avoid bias, dividing the dataset 5-fold each time. The average and standard deviation of these 100 training shuffles were computed below.

Table 4. Summary of the mean accuracies of 100 repeats.

	Accuracy	Recall	Precision	F1	Specificity
Mean	0.734597	0.749545	0.486601	0.58755	0.72953
STD	0.0351	0.0921	0.04608	0.0502	0.0502

3.2.5. Results(without outliers)

The same calculation and method were also applied on the data without the outliers, which increased the performance by ~%2.

Table 5. The result of the experiment (3.2.3) for the cleaned dataset.

	Accuracy	Recall	Precision	F1	Specificity
Fold-1	0.75581	0.81818	0.51428	0.63157	0.73437
Fold-2	0.72941	0.72727	0.48484	0.58181	0.73015
Fold-3	0.75000	0.57142	0.50000	0.53333	0.80952
Fold-4	0.69047	0.71428	0.42857	0.53571	0.68254
Fold-5	0.80952	0.80952	0.58620	0.68000	0.80952
Mean	**0.74704**	0.72813	0.50278	0.59248	0.75322
STD	0.03873	0.08886	0.050850	0.05660	0.04944

After clearing the outliers we randomly shuffled our dataset each time, divided it into 5-Folds, repeated it 100 times, and calculated the average and standard deviation of these 100 training tests so that there would be no bias during training and testing.

Table 6. Summary of the mean accuracies of 100 repeats.

	Accuracy	Recall	Precision	F1	Specificity
Mean	0.74869	0.75095	0.50363	0.59984	0.74793
STD	0.04788	0.09448	0.06632	0.06432	0.05978

According to the results of the area ratio rule based experiment, specific facial landmarks such as Po', Sn', A', Ls, Li, B', Pog', Gn', the area surrounding the Po' point at the level of the Li (Lower Lip) and the remaining area between Li' - Sn' - Po' (red zone in Fig-7) differs distinctly for skeletal Class-III malocclusion patients. The ratio method is an important distinguishing factor for Class-III classification; therefore, we decided to add it as a feature to our machine learning model.

medRxiv preprint doi: https://doi.org/10.1101/2022.07.26.22277593; this version posted July 27, 2022. The copyright holder for this preprint (which was not certified by peer review) is the author/funder, who has granted medRxiv a license to display the preprint in perpetuity.
All rights reserved. No reuse allowed without permission.

3.3. Machine Learning Approach

The machine learning method was performed in two main steps.

3.3.1) Extraction of orthodontic features from images.
3.3.2) The data set was labeled and the machine learning method is applied.

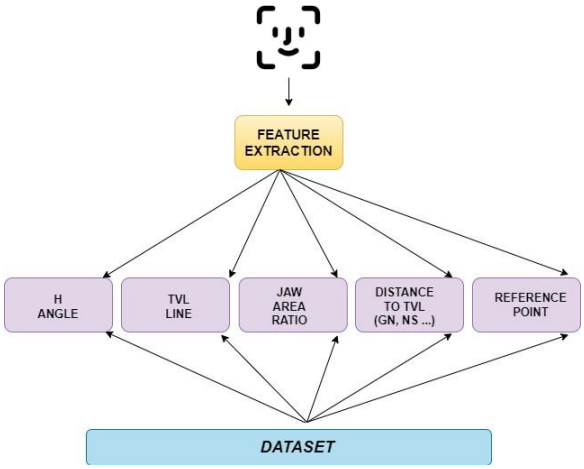

Figure 16. Extraction of orthodontic features from images.

3.3.1. Feature Extraction from Images

For calculation of H-Angle, we used the Python face-alignment library [15]. Firstly soft tissue nasion(N'), soft tissue chin(Pg') and upper lib(Ls) points (see Table 2) were computed. A line was drawn between Pg' and N' and a line between Pg' and Ls, and the angle between the lines passing through these points was calculated as in Fig-17.

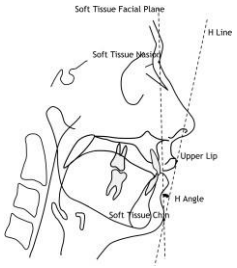

Figure 17. H-Angle of profile images.

To calculate the H angle in between, these points' x and y coordinate values were extracted as a 2- dimensional plane. With these coordinates, the slopes of these two lines were calculated using the formula in Fig- 18-b, and the angle H, which is the angle between the two lines, was calculated with the formula in Fig-18-a using these slopes.

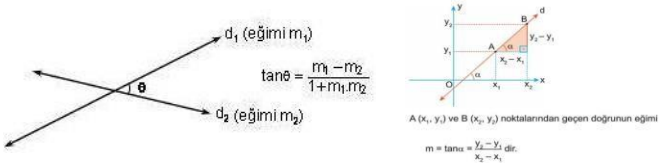

(a) (b)

Figure 18. (a) Angle between 2 points, (b) slope of a line.

The threshold value computed in section 3.2(rule based method) was incorporated as an additional feature.

For TVL line feature, 68 reference points on the face were computed as x and y values by drawing a parallel line to the Sn (Subnasale) point and perpendicular to the transverse plane.

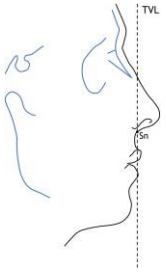

Figure 19. True Vertical Line (TVL).

The distances of each point to the TVL line were computed, and distance ratios were calculated as taking the TVL line as a reference. We aimed for a correct diagnosis from profile pictures taken by any mobile phone, but general variables of the images such as proximity, distance, location, and angle were not standard. . To achieve higher accuracy with the nonstandard photos, we decided that our machine learning model should handle the lengths of the points from the TVL as they were scalable. For this purpose, we scaled all the profile photos by dividing the distances between the landmark points by a reference length. To pick the best reference length to scale by, we experimented with all paired combinations of 68 points. As a result, when the TVL was divided by the length between G and Gn, the most accurate distance to TVL scaling was obtained. The distances between the "Gn'", "Sn'", "A'", "UL'", "LL'", "B'" and "Pog'" points on the face and the TVL were computed.

medRxiv preprint doi: https://doi.org/10.1101/2022.07.26.22277593; this version posted July 27, 2022. The copyright holder for this preprint (which was not certified by peer review) is the author/funder, who has granted medRxiv a license to display the preprint in perpetuity.
All rights reserved. No reuse allowed without permission.

3.3.2. Machine Learning Model

Firstly, we divided our data set into 75% training and 25% testing. Next, we selected the most appropriate model and parameter optimization on 75% of the training data. We calculated the correlations for the features, evaluated the features' correlation against each other, and removed the "Pog" data, as its correlation was greater than 0.80. No data was removed since we created our dataset by feature extraction from images.

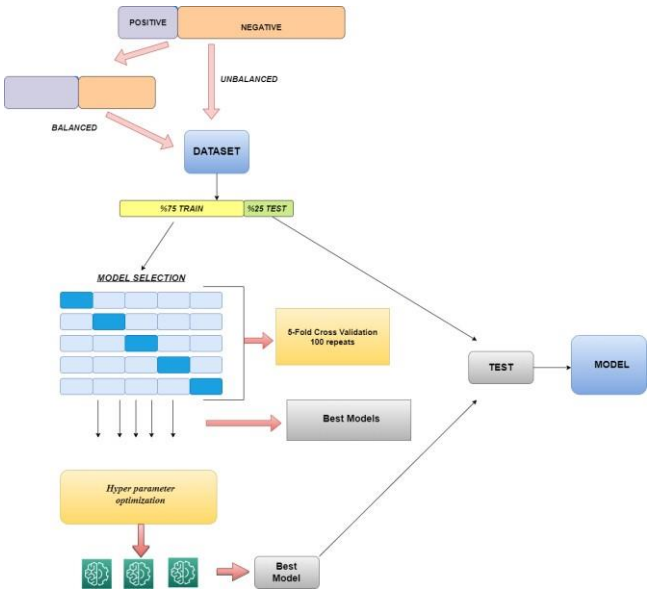

Figure 20. Experimental set-up for Machine Learning.

Since the data set, we used in the machine learning method was not balanced, we created a balanced data set with random selection of the negative class and kept the entire positive class. We compared the results by repeating the experiment twice for our balanced (Table-6) and unbalanced data sets (Table-7). In this experiment, we used 5-fold cross-validation for model selection and repeated this experiment 100 times on 18 models (Fig-20). We selected the model with the best results after the cross-validation. After hyperparameter optimization, the best parameters were selected. By creating our models according to these parameters, we tested them on the test data and selected the model with the best results.

Table 7. Balanced dataset results

	Accuracy	Precision	Recall	F1	AUC
LR	0.759 (0.071)	0.753 (0.084)	0.781 (0.115)	0.761 (0.076)	0.841 (0.065)
RC	0.765 (0.069)	0.754 (0.080)	0.796 (0.101)	0.770 (0.069)	0.842 (0.065)
SGD	0.681 (0.094)	0.739 (0.150)	0.684 (0.260)	0.658 (0.144)	0.836 (0.073)
PAC	0.604 (0.097)	0.689 (0.200)	0.692 (0.335)	0.595 (0.171)	0.822 (0.073)
KNNC	0.742 (0.068)	0.729 (0.076)	0.779 (0.103)	0.748 (0.069)	0.800 (0.069)
DT	0.656 (0.075)	0.661 (0.092)	0.641 (0.120)	0.644 (0.087)	0.653 (0.076)
ETC	0.653 (0.082)	0.660 (0.096)	0.652 (0.123)	0.651 (0.088)	0.652 (0.084)
L-SVC	0.754 (0.070)	0.754 (0.085)	0.764 (0.126)	0.752 (0.077)	0.837 (0.065)
SVC	0.765 (0.071)	0.759 (0.085)	0.785 (0.104)	0.767 (0.073)	0.836 (0.067)
NB	0.732 (0.069)	0.795 (0.108)	0.645 (0.128)	0.701 (0.086)	0.802 (0.074)
ABC	0.682 (0.075)	0.685 (0.086)	0.683 (0.117)	0.678 (0.081)	0.730 (0.081)
BC	0.722 (0.071)	0.743 (0.093)	0.685 (0.117)	0.703 (0.087)	0.783 (0.076)
RF	0.773 (0.070)	0.788 (0.090)	0.760 (0.115)	0.765 (0.079)	0.829 (0.069)
ETSC	0.773 (0.069)	0.788 (0.085)	0.751 (0.105)	0.765 (0.074)	0.824 (0.069)
GPC	0.769 (0.070)	0.736 (0.075)	0.847 (0.091)	0.784 (0.066)	0.815 (0.072)
GBC	0.728 (0.070)	0.735 (0.085)	0.726 (0.111)	0.723 (0.075)	0.790 (0.072)
LDA	0.730 (0.072)	0.736 (0.084)	0.726 (0.112)	0.725 (0.078)	0.815 (0.070)
QDA	0.657 (0.068)	0.757 (0.125)	0.482 (0.151)	0.571 (0.115)	0.756 (0.076)

Table 8. Unbalanced dataset results.

	Accuracy	Precision	Recall	F1	AUC
LR	0.825 (0.037)	0.722 (0.114)	0.510 (0.106)	0.591 (0.095)	0.859 (0.047)
RC	0.816 (0.032)	0.747 (0.125)	0.423 (0.106)	0.531 (0.099)	0.859 (0.047)
SGD	0.776 (0.100)	0.638 (0.175)	0.581 (0.224)	0.570 (0.106)	0.852 (0.050)
PA	0.661 (0.220)	0.579 (0.299)	0.455 (0.362)	0.372 (0.189)	0.845 (0.056)
KN	0.794 (0.042)	0.616 (0.108)	0.519 (0.117)	0.556 (0.095)	0.772 (0.060)
DT	0.733 (0.049)	0.473 (0.102)	0.491 (0.123)	0.475 (0.098)	0.654 (0.065)
ETC	0.725 (0.051)	0.458 (0.104)	0.469 (0.126)	0.451 (0.104)	0.638 (0.063)
L-SVC	0.824 (0.035)	0.733 (0.117)	0.483 (0.108)	0.577 (0.093)	0.858 (0.047)
SVC	0.819 (0.033)	0.729 (0.121)	0.466 (0.108)	0.560 (0.096)	0.853 (0.046)
NB	0.794 (0.047)	0.629 (0.126)	0.517 (0.134)	0.553 (0.097)	0.810 (0.059)
ABC	0.772 (0.041)	0.560 (0.103)	0.480 (0.119)	0.510 (0.097)	0.768 (0.068)
BC	0.779 (0.042)	0.597 (0.116)	0.441 (0.113)	0.499 (0.098)	0.784 (0.057)
RF	0.794 (0.037)	0.624 (0.102)	0.471 (0.114)	0.525 (0.097)	0.814 (0.054)

medRxiv preprint doi: https://doi.org/10.1101/2022.07.26.22277593; this version posted July 27, 2022. The copyright holder for this preprint (which was not certified by peer review) is the author/funder, who has granted medRxiv a license to display the preprint in perpetuity. All rights reserved. No reuse allowed without permission.

ETS C	0.792 (0.038)	0.617 (0.107)	0.467 (0.117)	0.528 (0.095)	0.802 (0.054)
GPC	0.810 (0.039)	0.680 (0.122)	0.485 (0.108)	0.558 (0.097)	0.819 (0.054)
GB	0.788 (0.041)	0.606 (0.110)	0.482 (0.116)	0.530 (0.098)	0.805 (0.055)
LD	0.814 (0.040)	0.689 (0.121)	0.499 (0.109)	0.571 (0.098)	0.842 (0.050)
QD A	0.759 (0.036)	0.560 (0.201)	0.253 (0.151)	0.326 (0.145)	0.783 (0.062)

As the Random Forest, Logistic regression, Ridge Classifier, Extra Trees Classifier, Linear SVM performed best, and we optimized the parameters on these five models to select the most optimal parameters. In addition, we applied parameter optimization on a few more models with close cross validation performances.

3.3.3. Hyper parameter optimization

We made hyperparameter optimization over the selecting models.

Table 9. Hyperparameter optimization results for four models.

Random Forest
'max_depth': 20
'max_features': 'auto'
'min_samples_leaf': 1
'n_estimators': 200

Gradient Boosting
'max_depth': 20
'max_features': 'auto'
'min_samples_leaf': 1
'n_estimators': 200

Logistic Regression
'C': 10
'penalty': 'l2'
'solver': 'newton-cg'

Ridge Classifier
'alpha': 0.1

3.3.4. Testing of Critical Models

Table 10: Balanced data test results for each model.

Random Forest Classifier	
Accuracy	**0.6727272727272727**
Precision	**0.6666666666666666**
F1	**0.689655172413793**
Recall	**0.7142857142857143**
AUC	**0.6719576719576721**
Gradient Boosting Classifier	
Accuracy	**0.7636363636363637**
Precision	**0.7586206896551724**
F1	**0.7719298245614034**
Recall	**0.7857142857142857**
AUC	**0.7632275132275131**
Ridge Classifier	
Accuracy	**0.7636363636363637**
Precision	**0.7419354838709677**
F1	**0.7796610169491526**
Recall	**0.8214285714285714**
AUC	**0.7625661375661377**
Linear SVC	
Accuracy	**0.7636363636363637**
Precision	**0.7586206896551724**
F1	**0.7719298245614034**
Recall	**0.7857142857142857**
AUC	**0.7632275132275131**
Logistic Regression	
Accuracy	**0.7636363636363637**
Precision	**0.7419354838709677**
F1	**0.7796610169491526**
Recall	**0.8214285714285714**
AUC	**0.7625661375661377**

Table 11: Unbalanced data test results for each model

Logistic Regression	
Accuracy	**0.7981651376146789**
Precision	**0.625**
F1	**0.576923076923077**
Recall	**0.5357142857142857**
AUC	**0.7123015873015872**
Random Forest Classifier	
Accuracy	**0.7981651376146789**
Precision	**0.6363636363636364**
F1	**0.56**
Recall	**0.5**
AUC	**0.7006172839506173**
Gradient Boosting Classifier	
Accuracy	**0.8256880733944955**
Precision	**0.68**
F1	**0.6415094339622641**
Recall_	**0.6071428571428571**
AUC	**0.7541887125220458**
Ridge Classifier	
Accuracy	**0.8348623853211009**
Precision	**0.7777777777777778**
F1	**0.6086956521739131**
Recall	**0.5**
AUC	**0.7253086419753088**
Linear SVC	
Accuracy	**0.8165137614678899**
Precision	**0.6818181818181818**
F1	**0.6**
Recall	**0.5357142857142857**
AUC	**0.724647266313933**
Extra Trees Classifier	
Accuracy	**0.8348623853211009**
Precision	**0.75**
F1	**0.6250000000000001**
Recall	**0.5357142857142857**
AUC	**0.7369929453262786**

Although the unbalanced dataset resulted in higher accuracy, F1 and precision were low. Therefore, balanced dataset's accuracy, F1 and recall score more represent the actual production accuracy. The best result for the balanced machine learning model was Logistic Regression with 76% accuracy, 74% precision and 77% F1, 82% recall, and AUC of 76%.

medRxiv preprint doi: https://doi.org/10.1101/2022.07.26.22277593; this version posted July 27, 2022. The copyright holder for this preprint (which was not certified by peer review) is the author/funder, who has granted medRxiv a license to display the preprint in perpetuity.
All rights reserved. No reuse allowed without permission.

4. Conclusion

This study presents the first fully automated machine learning method to accurately diagnose Class-III malocclusion applied across mobile images, to the best of our knowledge. For this purpose, we comparatively evaluated three machine learning approaches. We achieved 70% accuracy with the deep learning method, 74% accuracy with the area ratio method and 76% success with the machine learning method.

All three of our methods are flexible to be adapted to any dynamic training set of profile images of any ethnicity and age. Our next goal is to integrate our most accurate learning model among these three into a mobile application for parents and pediatricians seeking a second opinion on whether to reach out to an orthodontist at an early stage of developmental bone growth with a warning of Class-III malocclusion risk.

5. Acknowledgment

We want to thank Gül Sude Demircan, who developed the previous prototype, and Tülay Sevinç, who assisted in collecting the patient images and the consent forms.

6. References

[1] Staudt CB, Kiliaridis S. "Different skeletal types underlying Class-III malocclusion in a random population." Am J Orthod Dentofacial Orthop, 136(5), 715-721, 2009.

[2] Oltramari-Navarro PV, de Almeida RR, Conti AC, Navarro Rde L, de Almeida MR, Fernandes LS. "Early treatment protocol for skeletal Class-III malocclusion." Braz Dent J. ,24(2), 167-173, 2013.

[3] Al-Khalifa, Hussein. (2014). "Orthopedic Correction of Class-III Malocclusions during Mixed Dentition." Open Journal of Stomatology. 04(07), 372-380,2014

[4] Mandall N, Cousley R, DiBiase A, Dyer F, Littlewood S, Mattick R, Nute SJ, Doherty B, Stivaros N, McDowall R, Shargill I, Worthington HV. "Early Class-III protraction facemask treatment reduces the need for orthognathic surgery: a multi-centre, two-arm parallel randomized, controlled trial." J Orthod., 43(3), 164-175, 2016.

[5] Sharma JN. "Epidemiology of malocclusions and assessment of orthodontic treatment need for the population of eastern Nepal." World J Orthod., 10(4), 311- 316, 2009.

[6] X. Xu et al., "Advances in Smartphone-Based Point-of-Care Diagnostics," in Proceedings of the IEEE, vol. 103, no. 2, pp. 236-247, Feb. 2015, doi: 10.1109/JPROC.2014.2378776.

[7] Digital around the world - datareportal – global digital insights. DataReportal. (n.d.). Retrieved July 25, 2022, from https://datareportal.com/global-digital-overview

[8] Mobile Health Industry Trends and forecast 2021. Artezio. (n.d.). Retrieved July 24, 2022, from https://www.artezio.com/pressroom/blog/mobile-industry-forecast/

[9] Gupta G, Vaid NR. "The World of Orthodontic apps." APOS Trends Orthod, 7(2), 73, 2017.

[10] Development, C. S. (n.d.). Dental4Windows. Download.com. Retrieved July 24, 2022, from https://download.cnet.com/Dental4Windows/3000-2129_4-76472046.html

[11] Baheti, M.J., Toshniwal, N. "Orthodontic apps at fingertips.", Progress in Orthodontic, 15(1), 36, 2014.

[12] Phimentum. (n.d.). Retrieved July 23, 2022, from https://www.phimentum.com/

[13] Demircan, G.S., Kılıç, B., Önal-Süzek, T. (2021). "Early Diagnosis and Prediction of Skeletal Class-III Malocclusion from Profile Photos Using Artificial Intelligence." In: Jarm, T., Cvetkoska, A., Mahnič-Kalamiza, S., Miklavcic, D. (eds) 8th European Medical and Biological Engineering Conference. EMBEC 2020. IFMBE Proceedings, 80, 434-448, 2020.

[14] Basciftci,F.A.,Uysal,T.,Buyukerkmen,A."Determinati on of Holdaway soft tissue norms in Anatolian Turkish adults" Am J Orthod Dentofacial Orthop, 123(4),395-400, 2003.

[15] 1adrianb. (n.d.). 1adrianb/face-alignment: 2D and 3D face alignment library build using pytorch. GitHub. Retrieved July 24, 2022, from https://github.com/1adrianb/face-alignment.

Appendix

LR	Logistic Regression
RC	Ridge Classifier
SGD	SGD Classifier
PA	Passive Aggressive Classifier
KN	K Neighbors Classifier
DT	Decision Tree Classifier
ETC	Extra Tree Classifier
L-SVC	Linear SVC
SVC	SVC
NB	Gaussian NB
ABC	Ada Boost Classifier
BC	Bagging Classifier
RF	Random Forest Classifier
ETSC	Extra Trees Classifier
GPC	Gaussian Process Classifier
GB	Gradient Boosting Classifier
LD	Linear Discriminant Analysis
QDA	Quadratic Discriminant Analysis